International Journal of Microwave and Wireless Technologies

cambridge.org/mrf

A MOEA/D-IHPSO-based multi-objective optimization for dual-polarized omnidirectional antenna design

Jiangling Dou[1,2], Cailong Zhong[2], Dan Li[2], Jian Song[2] and Tao Shen[3]

[1]Yunnan Key Laboratory of Computer Technologies Application, Kunming University of Science and Technology, Kunming, China; [2]Information Engineering and Automation, Kunming University of Science and Technology, Kunming, China and [3]Yunnan Vocational College of Mechanical and Electrical Technology, Kunming, China

Research Paper

Cite this article: Dou J, Zhong C, Li D, Song J, Shen T (2026) A MOEA/D-IHPSO-based multi-objective optimization for dual-polarized omnidirectional antenna design. *International Journal of Microwave and Wireless Technologies* **18**(5), 759–769. https://doi.org/10.1017/S1759078726103171

Received: 31 October 2025 UTC
Revised: 5 April 2026 UTC
Accepted: 13 April 2026 UTC
First published online: 7 August 2026 UTC

Keywords:
dual-polarized omnidirectional antenna; Multi-objective; topology optimization; transfer learning

Corresponding author: Tao Shen; Email: shentao@kust.edu.cn

Abstract

A multi-objective evolutionary algorithm based on decomposition with an improved hybrid particle swarm optimization (MOEA/D-IHPSO) method is proposed, which aims to enhance the efficiency of automated optimization for antenna geometry. The optimization process includes two stages: optimization problem modeling and algorithm application. In the first stage, the topology optimization regions are selected according to the surface current distribution of the antenna, and a differential grid division strategy is employed to characterize the selected regions, ensuring the modeling accuracy of the key topology areas. By combining the encoded topological parameters of the selected regions with the key size parameters, a hybrid solution vector is formed and subsequently used to generate the initial population. In the second stage, the proposed framework uses new crossover and adaptive mutation operators to accelerate the process of reaching the target solution. Furthermore, MOEA/D-IHPSO incorporates a novel transfer learning-based recombination strategy that directly leverages historical optimization data without requiring surrogate model training, thereby intelligently guiding the search direction. To validate the effectiveness of the method, a dual-polarized omnidirectional antenna is optimized. Experimental results show that the optimization efficiency is improved by 31.8% and 26% compared to IBPSO and MOEA/D-GO algorithms, respectively.

Introduction

Traditional antenna design methods typically rely on prior knowledge to select a predetermined geometric configuration, and then the size parameters of the antenna are optimized based on design objectives such as isolation, reflection coefficient, and radiation characteristics. However, traditional antenna design schemes are time-consuming and limited in design flexibility. To improve the optimization efficiency of antennas and explore more novel topology structures, antenna topology optimization methods have emerged [1–3].

Existing topology optimization methods mainly fall into two categories: gradient-based algorithms and evolutionary algorithm-assisted methods. Gradient-based topology optimization methods [4–6] rely on sensitivity analysis to obtain the gradient information of the objective function, which is used to guide the adjustment of elements in the antenna geometry. However, this type of method requires an accurate finite element (FE) model and suitable material interpolation functions, a requirement that is challenging for complex antenna structures and limits the generalization ability of such approaches. Compared with gradient-based optimization algorithms, evolutionary algorithm-driven antenna topology optimization methods [7–11] do not rely on gradient information, while the optimal geometric structure is searched through the simulation of natural selection and genetic mechanisms. These methods are usually combined with multi-objective evolutionary algorithms [12] and binary particle swarm optimization (BPSO) algorithms [13] to solve multi-objective optimization problems. However, the computational cost of evolutionary algorithm-assisted optimization methods is relatively high, so improving optimization efficiency is one of the main challenges.

In order to improve the optimization efficiency of antennas, researchers have proposed methods based on offspring reproduction (OR) and fitness allocation (FA) to optimize antenna design. OR-based optimization methods mainly include Gaussian process regression [14], surrogate model-assisted optimization [15–17], and simulation-driven surrogate parallel improved adaptive genetic algorithm [18], which effectively enhance topology optimization efficiency. However, these methods incur high computational costs for constructing high-precision surrogate models. FA-based optimization methods mainly rely on high-fidelity surrogate models such as space mapping and neural networks [19–21] to reduce the number of EM simulations,

© The Author(s), 2026. Published by Cambridge University Press in association with The European Microwave Association.

but a trade-off between antenna optimization efficiency and the quality of the agent model is a major challenge.

To address key challenges in current antenna optimization, such as the difficulty in balancing multiple objectives, the limited design freedom of sequential optimization approaches, the tendency of conventional evolutionary algorithms to converge to local optima, and high computational costs, a novel optimization framework MOEA/D-IHPSO, is proposed in this paper. It integrates the multi-objective evolutionary algorithm with an improved hybrid particle swarm optimization. The main contributions are as follows.

1) A unified hybrid encoding scheme integrating discrete topological and continuous size parameters is established. In addition, a differentiated grid-division strategy based on surface current distribution is introduced to balance search efficiency and design accuracy.
2) A hybrid crossover strategy and a new adaptive mutation operator are combined to dynamically coordinate global and local search, effectively mitigating the issue of premature convergence.
3) A transfer learning-driven recombination mechanism without surrogate model training is proposed, which guides the search direction by directly recombining high-performance modules from historical optimization data.

This comprehensive approach achieves the coordinated optimization of both the topology and key dimensions of the antenna, while simultaneously improving optimization efficiency and design flexibility. A dual-polarized omnidirectional antenna is designed with this method. Experimental results demonstrate that the operating bandwidth is significantly expanded, port isolation and omnidirectionality are improved, and the optimization time is notably reduced compared to the IBPSO and MOEA/D-GO methods.

Proposed method

Optimization process of the proposed method

The collaborative optimization framework of the MOEA/D-IHPSO method for efficiently enhancing and balancing multiple performance metrics of the initial antenna design is shown in Fig. 1. First, in the optimization problem modeling phase, a multi-objective function is designed according to the multiple performance index requirements of the antenna. Guided by the surface current distribution as electromagnetic physical prior knowledge, the key regions on the upper and lower radiating patches are selected for optimization. A differentiated network partitioning strategy is used to map the two selected antenna design spaces to binary topology parameter arrays $X_1 = [x_1, x_2, \ldots, x_m]$ and $X_2 = [x_1, x_2, \ldots, x_n]$. At the same time, the key size parameters $G_q = [g_1, g_2, .., g_q]$ with the most significant impact on antenna performance are identified using methods such as surface current analysis, equivalent circuit modeling, or sensitivity analysis. The selected topological and size parameters serve as the optimization design variables of the antenna, together forming a hybrid solution vector that establishes a unified search space for concurrent optimization. After defining the population size, Latin Hypercube Sampling [14] is used to generate the initial population within the defined solution space, laying the foundation for subsequent optimization iterations. Second, in the algorithm application phase, the proposed framework integrates evolutionary and swarm intelligence principles. For the top 50% of individuals in the fitness ranking, a hybrid crossover strategy combining single-point and multi-point crossover is applied to the topology parameters, while simulated binary crossover is used for the size parameters. For the remaining individuals, the improved hybrid particle swarm optimization (IHPSO) guides the updates, wherein an adaptive mutation operator is embedded to dynamically balance global and local search by adjusting the mutation probability according to the fitness convergence status. To further improve search efficiency, a transfer learning-driven recombination strategy is incorporated. It is automatically activated when the convergence rate drops significantly or a specified number of generations is reached, thereby continuously advancing the search for the optimal solution. The optimization process terminates upon reaching the preset iteration limit or meeting multiple preset goals, and the final Pareto optimal solution set is output as the preferred solution for the joint design of antenna topology and size parameters.

Objective function design

The design of high-performance antennas requires a rigorous multi-objective optimization framework to simultaneously improve multiple key electromagnetic (EM) performance metrics. The return loss, isolation between the two ports, omnidirectionality, and gain flatness are used as optimization objectives in this paper. The optimization problem is transformed into the following mathematical expression to guide the algorithm in fully exploring the optimal performance of the antenna.

$$\min_{Z} F(Z) = (f_1(Z), f_2(Z), f_3(Z), f_4(Z), f_5(Z)) \quad s.t.\ Z \in \Omega \tag{1}$$

The variable Z is the decision variable of the topology parameters X and the size parameters G_q, while Ω denotes the design space. For ports 1 and 2, to ensure that the return loss is greater than C_1 (dB) within the operating frequency band $[\omega_1, \omega_2]$, the objective functions $f_1(Z)$ and $f_2(Z)$ are defined as follows.

$$f_i(Z) = \max(C_1 - \min_{\omega \in [\omega_1, \omega_2]} |S_{ii}(Z, \omega)|, 0) \cdot (1 + \gamma) \tag{2}$$

$i = 1$ and 2. In order to suppress mutual coupling between the two ports and ensure that the isolation of the optimized antenna is higher than C_2 (dB), the objective function $f_3(Z)$ is defined as follows.

$$f_3(Z) = \max(C_2 - \min_{\omega \in [\omega_1, \omega_2]} |S_{21}(Z, \omega)|, 0) \cdot (1 + \gamma) \tag{3}$$

γ is the penalty factor. Within the operating frequency range, when $\min|S_{ii}|$ is below C_1 dB or $\min|S_{21}|$ is below C_2 dB, the penalty value is linearly proportional to the exceeding amplitude. Additionally, to ensure that the optimized antenna has satisfactory omnidirectional radiation characteristics at multiple key frequency points, the omnidirectional fluctuation objective function f_4(Z) is defined as follows.

$$f_4(Z) = \max(f_4(Z)|_{f_1}, f_4(Z)|_{f_2})$$
$$f_4(Z)|_{f_i} = \max([\max_{\varphi} G(Z, f_i, \varphi, \theta_0) - \min_{\varphi} G(Z, f_i, \varphi, \theta_0)] - C_3, 0) \tag{4}$$

$G(Z, f_i, \varphi, \theta_0)$ represents the realized gain evaluated at frequency f_i, azimuth angle φ, and a fixed elevation angle θ_0, while C_3 denotes the threshold for omnidirectional performance. To further improve the performance stability of the antenna within the operating frequency band and suppress fluctuations in the

https://doi.org/10.1017/S1759078726103171 Published online by Cambridge University Press

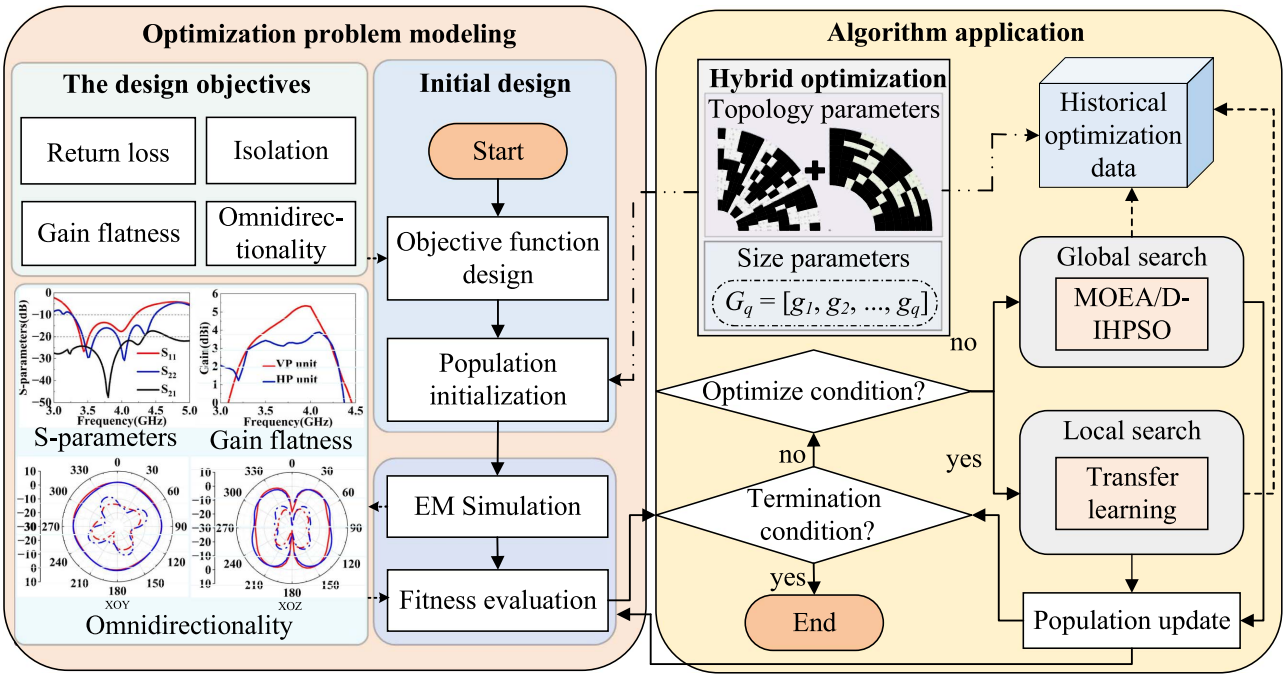


Figure 1. Overall optimization process flow of MOEA/D-IHPSO.

gain-frequency response curve, the gain-flatness objective $f_5(Z)$ is defined as follows.

$$f_5(Z) = \max([\max_{\omega\in[\omega_1,\omega_2]} G(Z,\omega) - \min_{\omega\in[\omega_1,\omega_2]} G(Z,\omega)] - C_4, 0) \quad (5)$$

$G(Z,\omega)$ represents the realized gain within the operating frequency band. C_4 is the threshold for the gain flatness level. A smaller $f_5(Z)$ indicates a more stable antenna gain.

For an antenna to operate in a frequency band ranging from 3.3 to 4.1 GHz, the objective function is specified by setting (ω_1, ω_2) = (3.3 GHz, 4.1 GHz) and (C_1, C_2) = (10 dB, 20 dB), so that the optimized antenna attains a return loss better than 10 dB and an isolation better than 20 dB. As a gain variation of less than 3 dB is widely recognized as indicative of excellent omnidirectional performance and stable gain [22, 23], C_3 and C_4 are set to 3 dB to ensure that the antenna design meets this standard. Furthermore, to guarantee the performance at key frequencies within the band, f_1 and f_2 are set to 3.5 and 3.8 GHz, respectively. The optimization range for the key size parameter h is set to 5–10 mm, which is determined by combining theoretical considerations of the coupling length [24] with systematic parametric sweep results. R_7 is set to 1–4 mm to ensure mechanical compatibility with standard metric screws for manufacturability.

Topology optimization region division strategy based on current distribution characteristics

Based on the lightweight and easily integrable nature of planar fragmented structures (FTS), the MOEA/D-IHPSO algorithm is employed to search for the optimal topological distribution of FTS within the refined unit design space. According to the surface current distributions on the upper and lower radiating patches, regions with significant current-intensity variation are selected for optimization. Meanwhile, to avoid geometric defects introduced by sector discretization, a circular patch is preset in the design. The selected optimization region is shown as the shaded area in Fig. 2. To further implement the structured grid division, the selected region is divided into four equal sectors by two perpendicular dashed lines passing through the circle center, as shown in Fig. 3. One sector is discretized into sector-ring unit cells in polar coordinates and mapped onto the binary design matrix. "1" represents a metal unit cell and "0" represents a non-metal unit cell. This novel physics-informed binary encoding interface is crucial for balancing design accuracy and optimization efficiency, while reducing error accumulation. Finally, the complete radiation patch is obtained by mirroring and rotating operations to ensure structural symmetry, which is fundamental for achieving the desired omnidirectional radiation pattern.

After selecting the optimization region, two efficient mesh division strategies are proposed based on the current-distribution characteristics of the selected area (Fig. 2) to further enhance design flexibility. The current in the upper structure shows a distinct edge accumulation characteristic, so a non-uniform angular partitioning strategy is applied to this region. Specifically, the sectorial optimization region is evenly divided into 8 annular layers to balance modeling accuracy and the number of optimization variables. The angular direction is divided into 10 equal parts near the axis, while the edge region where the current intensity changes more significantly is divided into 20 equal parts to achieve refined optimization of the key areas, as shown in Fig. 3(a). The current distribution in the lower structure is more uniform, so an equal-area meshing strategy is adopted, as shown in Fig. 3(b). In this approach, the angular direction is divided into 10 equal parts, and the radial direction is partitioned into 8 layers with proportionally scaled boundaries to ensure that each sector ring unit has an equal area. This results in a moderately sized 8 × 10 grid that balances optimization across the region and enhances manufacturability. The combination of these two strategies not only helps suppress the accumulation of discrete errors in topology optimization, but

https://doi.org/10.1017/S1759078726103171 Published online by Cambridge University Press

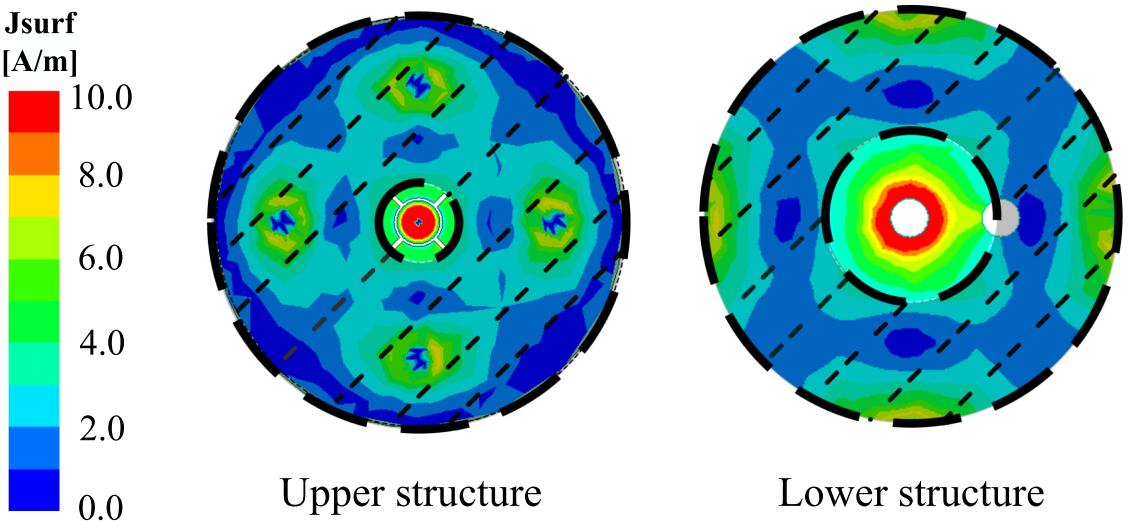


Figure 2. Current distribution and optimization region.

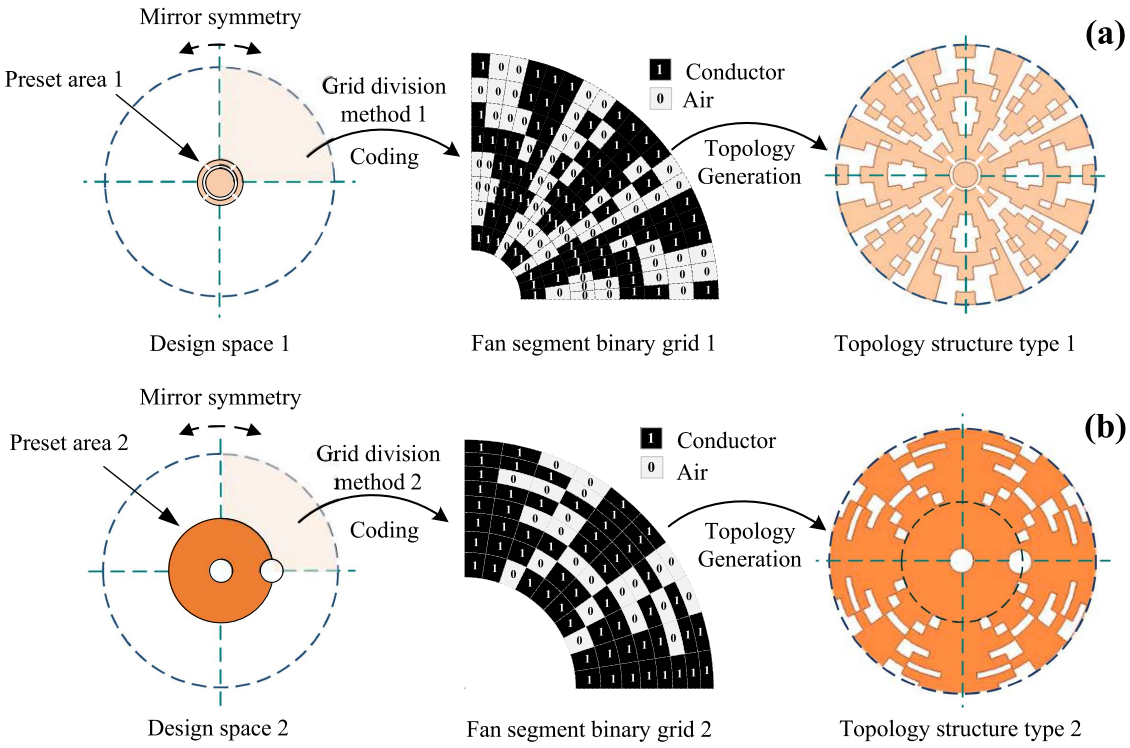


Figure 3. Two network partitioning strategies and binary encoding of topological structures. (a) Non-uniform angular partitioning network and (b) equal area sector partitioning network.

also ensures design accuracy and practical feasibility during the optimization process, thereby improving the overall optimization effect.

Improved HPSO

To address the joint optimization problem of topology and size parameters, this study proposes an IHPSO algorithm. This algorithm combines BPSO and continuous particle swarm optimization for the joint optimization of discrete topology parameters and continuous size parameters within a unified coding framework. A mixed encoding scheme is employed for each particle, in which the topology parameters are represented by 0/1 Boolean variables representing fragmented metal structures, and the size parameters are encoded as real numbers. After each update, the size parameters are rounded to one decimal place to satisfy manufacturing tolerance requirements. The topology parameters are updated using the sigmoid function in BPSO for probabilistic flipping, and the mapping function is given as follows.

$$S(v_k) = \frac{1}{1 + e^{-v}} \tag{6}$$

https://doi.org/10.1017/S1759078726103171 Published online by Cambridge University Press

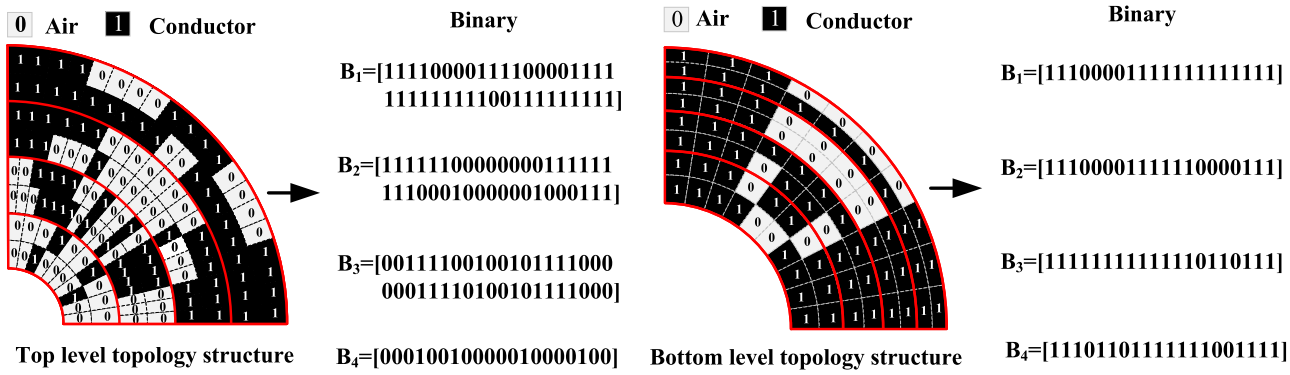


Figure 4. Schematic diagram of topology structure modularity.

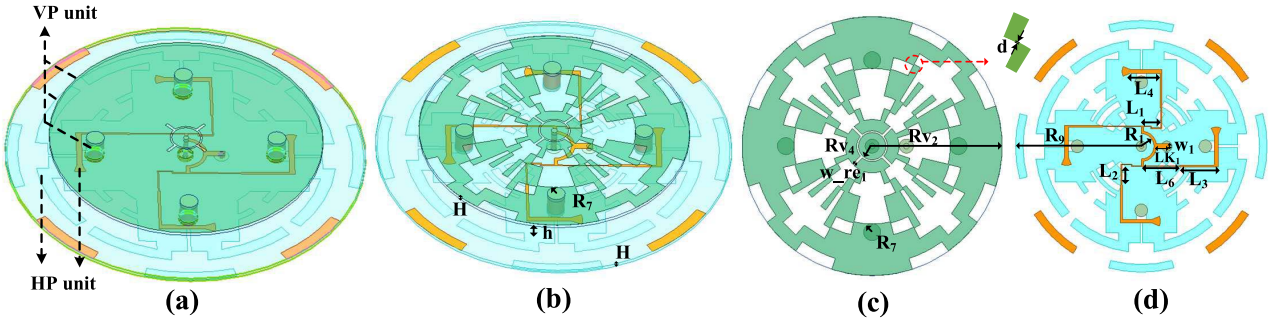


Figure 5. Initial and optimized structure of the dual-polarized omnidirectional antenna. $H = 1$, $h = 6$, $R_1 = 6$, $R_7 = 2.5$, $R_9 = 49.5$, $Rv_2 = 38$, $Rv_4 = 4.5$, $w_re_1 = 0.4$, $L_1 = 8$, $L_2 = 7.2$, $L_3 = 15$, $L_4 = 12$, $L_6 = 15.2$, $LK_1 = 6$, $W_1 = 2$, $d = 0.15$ (units: mm). (a) Initial structure, (b) optimized structure, (c) optimized upper layer, and (d) optimized lower layer.

v represents the velocity value of the current position of the particle, which is used to control the probability of topological site flipping.

Meanwhile, IHPSO introduces an adaptive mutation mechanism based on fitness to enhance population diversity and prevent premature convergence. The mutation probability P is dynamically adjusted according to the difference between the average aggregate fitness f_{av} of a few elite individuals in the previous generation and the fitness threshold f_{th}.

$$P = \begin{cases} P_{\max}, & f_{\text{av}} < f_{\text{th}} \\ P_{\min} + (P_{\max} - P_{\min}) \cdot (1 - \frac{f_{av} - f_{th}}{f_{av}}), & f_{\text{av}} \geqslant f_{\text{th}} \end{cases} \tag{7}$$

The mutation probability P is dynamically adjusted within a preset range $[P_{\min}, P_{\max}]$. If f_{av} falls below the threshold f_{th}, the mutation rate P is increased to enhance population diversity. After the mutation is triggered, the topological parameters and size parameters are differentially perturbed. The topological parameters undergo a Boolean flip operation on their elements with probability P. The size parameters are perturbed by adding a standard normal random term to the current position, thereby helping the search escape local optima in the continuous space. The improved operator dynamically adjusts the mutation strength according to the current search state, thus better balancing global search and local optimization and preventing the algorithm from getting stuck in local optima.

Transfer learning-driven recombination strategy

To further enhance the efficiency of automated antenna design, a transfer learning-driven joint recombination strategy for topology and size parameters is proposed. The transfer learning mechanism adopted by this strategy is different from the typical deep learning paradigm. It does not rely on model training, but instead achieves knowledge transfer and reuse by directly reorganizing and perturbing structural modules and parameters extracted from high-performing individuals in historical optimization runs. This mechanism aims to improve the quality and diversity of the population. The detailed procedure is as follows.

In the first step of the process, the fitness improvement rate $\Delta F^{(g)}$ is defined to monitor the evolutionary trend of the population.

$$\Delta F^{(g)} = \frac{F_{best}^{(g)} - F_{best}^{(g-1)}}{|F_{best}^{(g-1)}| + \varepsilon} \tag{8}$$

$F^{(g)}{}_{\text{best}}$ represents the optimal total fitness of the gth generation and ε is a small positive number set to 1×10^{-10} to ensure numerical stability. The transfer learning-driven recombination strategy is triggered when the algorithm detects convergence stagnation. Specifically, stagnation is identified if the fitness improvement rate remains below a predefined threshold for a specified number of consecutive generations.

$$\frac{1}{T}\sum_{k=1}^{T} \Delta F^{(g-k)} < \delta, \quad g > T \tag{9}$$

δ is the fitness improvement threshold and is set to 0.01 based on observations of the initial algorithm convergence rate. T is the

https://doi.org/10.1017/S1759078726103171 Published online by Cambridge University Press

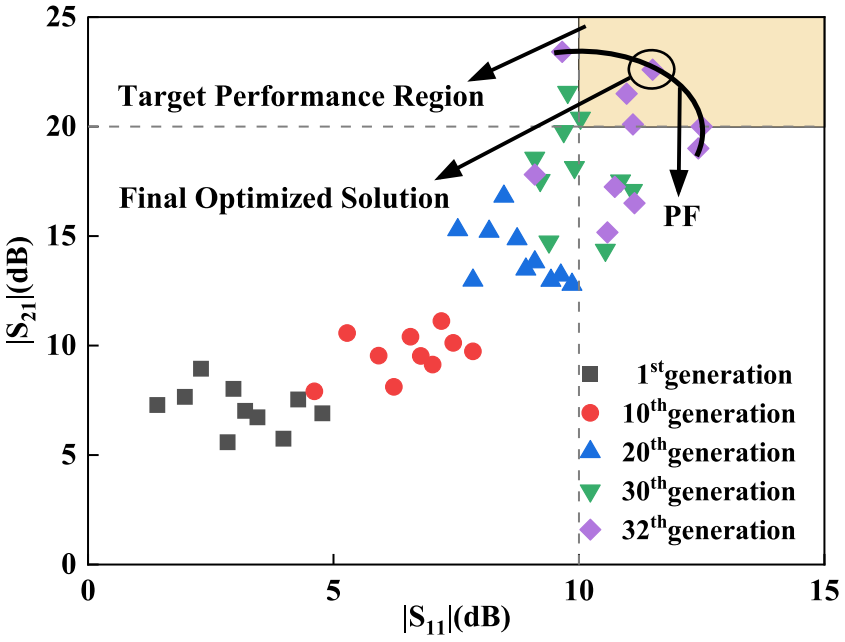


Figure 6. Pareto frontier solution and optimization process evolution.

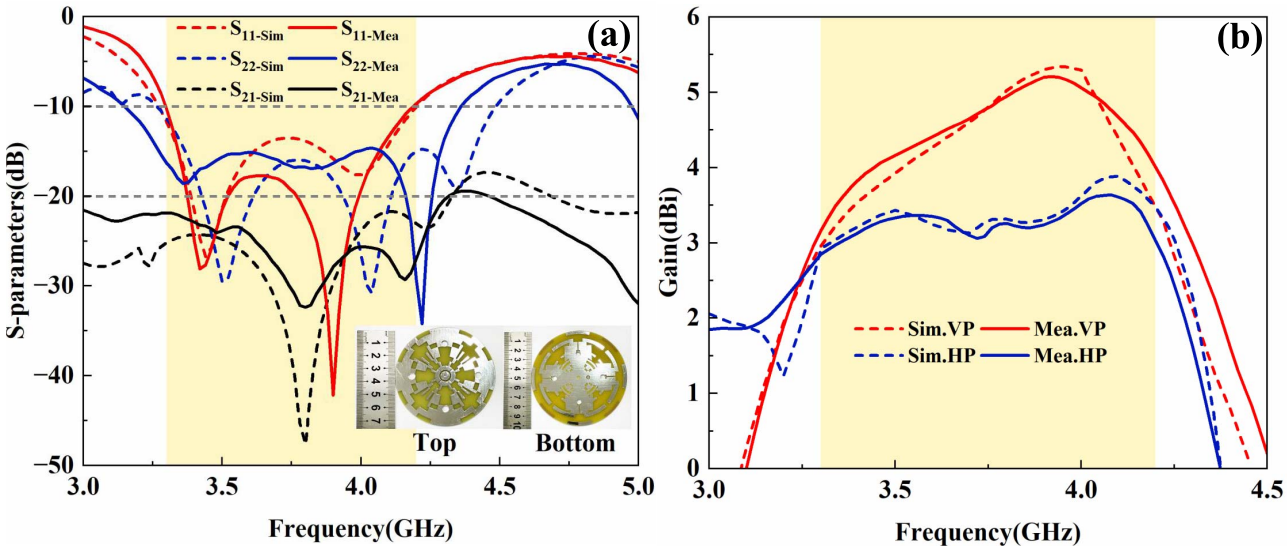


Figure 7. The simulated and measured results of the optimized antenna. (a) S-parameters and (b) peak gain.

number of consecutive stagnant generations and is empirically set to 5 to ensure reliable detection. Subsequently, the system selects the top N individuals (N is the current population size) from the historical optimization data based on the five indicators S_{11}, S_{22}, S_{21}, omnidirectionality, and gain flatness, respectively, to construct five distinct label pools T_{11}, T_{22}, T_{21}, T_o, and T_g. After the structural label is constructed, the individuals in the population can be expressed as follows.

$$I^{(i)} = \left\{ B_1^{(i)}, B_2^{(i)}, \ldots, B_n^{(i)}, G_q{}^{(i)} \right\} \tag{10}$$

$B_j{}^{(i)}$ represents the jth layer structure module in the ith individual topology structure. $G_q{}^{(i)}$ is the vector of q parameters associated with the individual $I^{(i)}$.

The strategy then performs splicing and recombination of the topological structures. The individuals in the label pool are uniformly divided into four structural modules (Fig. 4), forming four corresponding module pools. The strategy randomly selects one module from each module pool with equal probability and splices them into a new structural individual. If a module pool contains M modules, the probability of selecting any specific module from it is $1/M$.

$$B_{new} = [B_1{}^{(p)}, B_2{}^{(q)}, B_3{}^{(r)}, B_4{}^{(s)}] \tag{11}$$

p, q, r, and s are the indices for the four randomly selected modules.

Finally, parameter perturbation sampling is conducted to generate the size parameters for the newly recombined topology. The system first identifies the set S of all historical elite individuals that contribute modules to B_{new}. A new size parameter vector G_{new} is

https://doi.org/10.1017/S1759078726103171 Published online by Cambridge University Press

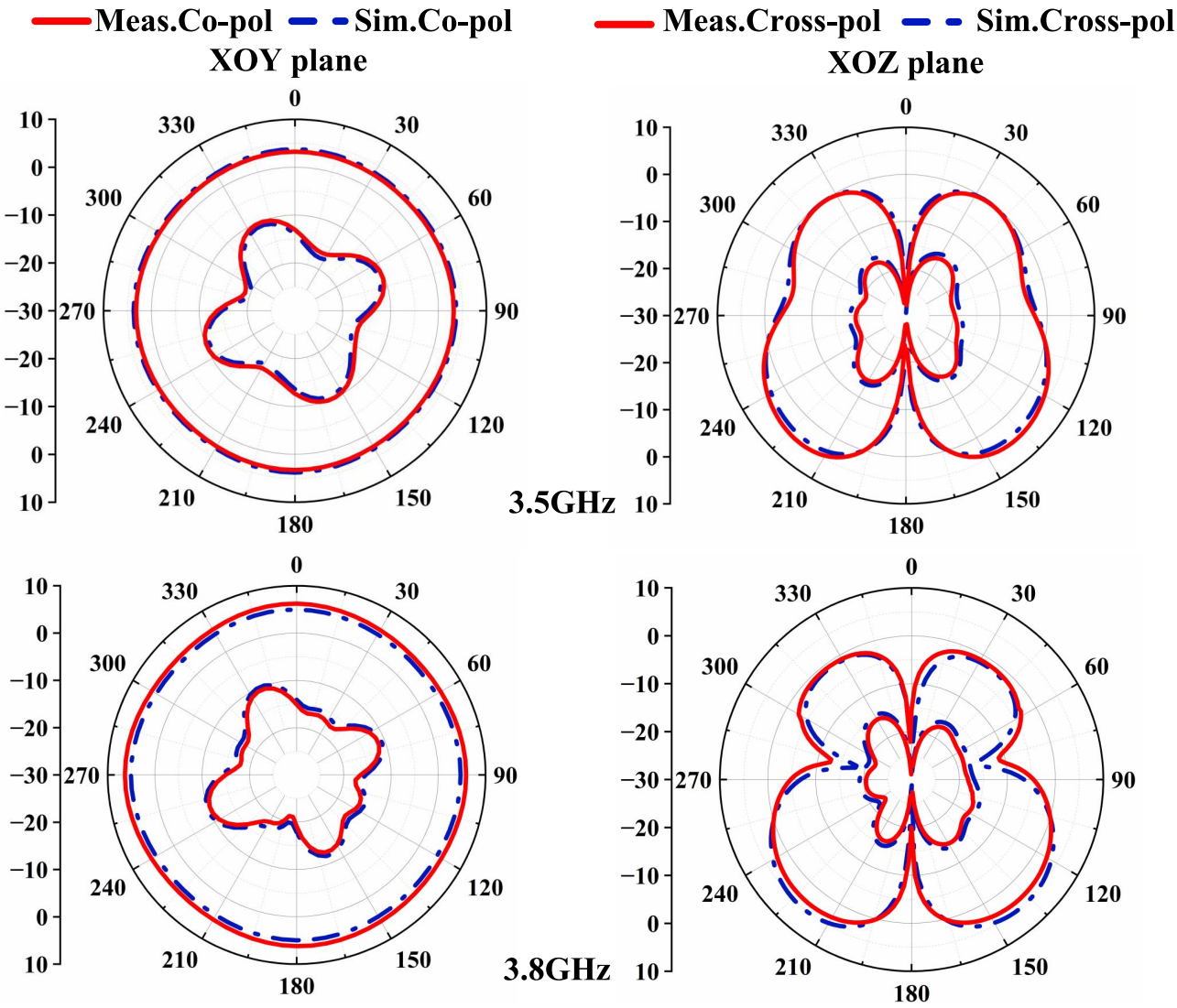


Figure 8. Measured and simulated gain patterns for the VP element at 3.5 and 3.8 GHz.

then generated by applying a Gaussian perturbation to the mean parameters according to the following formula.

$$G_{new} = \frac{1}{|S|}\sum_{I^{(i)}\in S} G_q^{(i)} + \eta \cdot \epsilon,\ \epsilon \in \mathrm{N}(0,\sigma^2\mathrm{I}) \qquad (12)$$

η is the perturbation coefficient, typically set to 0.1 to control the overall scale of exploration. The vector $\boldsymbol{\epsilon}$ is a multivariate Gaussian noise, where σ^2 defines its variance, usually set to a small fraction of the allowable parameter range. The identity matrix $\mathbf{I}$ ensures that the noise is added independently to each size parameter with equal variance. All generated parameter values are constrained to the feasible manufacturing range. This approach performs directed perturbation based on excellent parameter benchmarks, effectively utilizing historical experience while ensuring the diversity of the new parameters. The new topology B_{new} and its associated parameters G_{new} are concatenated to form a new candidate individual $I_{\text{new}} = [B_{\text{new}}, G_{\text{new}}]$. This process is repeated to generate the new population.

This strategy significantly enhances the directionality and diversity of the structural reconstruction process by integrating the triple mechanisms of structural label guidance, module reorganization, and parameter reorganization sampling, thereby effectively improving the overall convergence efficiency. This improvement is achieved with negligible computational overhead.

Analysis of experimental results

Introduction of the initial and optimized antenna structure

To verify the effectiveness of the proposed MOEA/D-IHPSO for antenna optimization, a dual-polarized omnidirectional antenna is optimized. The antenna structure consists of a vertical polarization (VP) unit and a horizontal polarization (HP) unit, and its initial configuration is shown in Fig. 5(a), which employs an FR-4 substrate with a relative permittivity of 4.4 and a loss tangent of 0.02. The optimized antenna configuration is shown in Fig. 5(b), with the optimal topological layouts of the upper and lower antenna layers presented in Fig. 5(c) and (d). The optimal values of h and R_7 are 6 and 2.5 mm, respectively. To ensure overall electrical continuity

https://doi.org/10.1017/S1759078726103171 Published online by Cambridge University Press

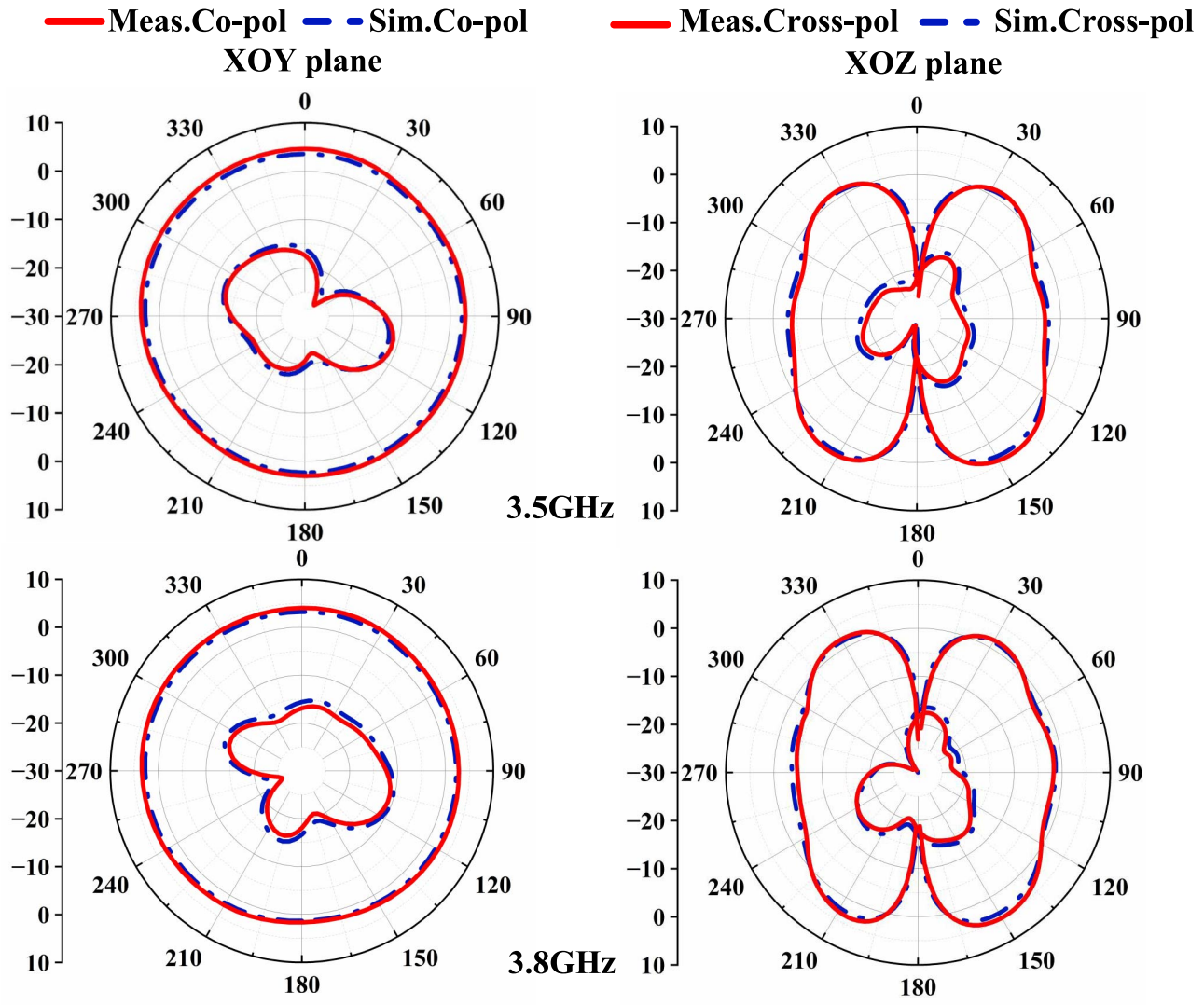


Figure 9. Measured and simulated gain patterns for the HP element at 3.5 and 3.8 GHz.

of the segmented structure, the edge length of each unit increases successively by 0.15 mm along the radial direction.

Experimental environment and optimization results

The entire simulation process is performed on a computer equipped with 128 GB of memory, an Intel Core i9–14900KS processor, and an NVIDIA GeForce RTX 5060 GPU. The simulation software is ANSYS HFSS 2022R1. To enable automated simulation, the binary-encoded topology matrix generated by the algorithm is programmatically converted into a standard CAD file, which is then imported into HFSS for full-wave electromagnetic analysis and performance evaluation. The optimized areas of the sector-shaped radiating patches on the upper and lower layers are discretized into 140 and 8 × 10 units. In MOEA/D-IHPSO, the initial population size N is set to 36 and the maximum number of iterations N_t is set to 50.

After 32 iterations of optimization, which correspond to 1152 full-wave solutions, the topology configuration of both design spaces and the size parameters h and R_7 are simultaneously converged. The bandwidth optimized by MOEA/D-IHPSO is from 3.27 to 4.2 GHz, with isolation above 20 dB across this frequency band. Moreover, the gain curve exhibits a smooth variation, and at the frequency points of 3.5 and 3.8 GHz, the gain fluctuation in the azimuth plane is less than 3 dB, which verifies the engineering feasibility of simultaneously optimizing both the topology and size parameters. The evolution trajectory of some representative solutions from the Pareto set is shown in Fig. 6. With optimization iterations, the solution population evolves from an initial random distribution to a high concentration in the target performance region. The majority of solutions in the final generation converge to the Pareto front, demonstrating the effective trade-off of the algorithm between reflection loss and isolation.

The proposed MOEA/D-IHPSO can be extended to other planar antenna designs, such as microstrip patch antennas and planar monopole antennas, where discrete topology patterns and continuous geometric parameters need to be optimized simultaneously for multiple performance objectives. In practice, the overall computational expense is still dominated by full-wave simulations, while the added cost of the evolutionary operators and transfer learning-driven recombination remains lightweight. Although the initial population is generated stochastically, sensitivity to initialization is

https://doi.org/10.1017/S1759078726103171 Published online by Cambridge University Press

Table 1. Comparison information with similar optimization algorithms

Ref.	Optimization method	Design space	Number of EM	Time	Optimized frequency (GHz)	Dimension (in λ_0)	Polarization
[25]	GA	16 × 16 pixels	1550	520.8 h	1.9–10	1.59 × 0.89 × 0.03	Single
[26]	TR-SADEA	23 params	1708	285.6 h	3.3–5	1.17 × 1.17 × 0.25	Single
[27]	MEA	10 × 14 pixels	3104	411.5 h	3.5–9.7	Not given	Dual
[28]	IMT + TD3	29 × 18 pixels	2787	115.6 h	2.37–2.47	0.48 × 0.48 × 0.01	Single
[29]	IBPSO	8 × 10 pixels	4590	119.1 h	2.4/3.5/5.8	0.43 × 0.24 × 0.01	Single
[30]	BBSO	20 × 20 pixels	2500	Not given	1.9–2.4	1.08 × 0.79 × 0.02	Single
[31]	MOEA/D-M	9 × 9 pixels	720	Not given	4.78–6.02	0.36 × 0.31 × 0.03	Dual
[32]	MOEA/D-GO	Top 8 × 9 Bottom 10 × 14 pixels	Not Given	148 h	1.7–3.8	1.19 × 1.19 × 0.43	Dual
[33]	MOEA/D-EOR	9 × 9 pixels	2232	98.4 h	4.95–5.07	0.67 × 0.67 × 0.001	Dual
This work	MOEA/D-IHPSO	Top 140 bottom 8 × 10 pixels + 2 params	1152	86.4 h	3.3–4.2	1.25 × 1.25 × 0.1	Dual

Note: λ_0 is the wavelength at the center frequency of the operation band.

mitigated by IHPSO and a recombination mechanism that injects high-quality modules from historical data.

Measurement and comparison

The measurement results of antenna

To verify the engineering effectiveness and optimization performance of the MOEA/D-IHPSO algorithm, the optimized dual-polarized omnidirectional antenna is experimentally tested. As shown in Fig. 7(a), the measured −10 dB impedance bandwidth is from 3.3 to 4.2 GHz. The peak gain values of the VP and HP units are shown in Fig. 7(b), with VP varying between 3.16 and 5.21 dBi, and HP varying between 2.85 and 3.64 dBi. The radiation patterns of the designed antenna at several frequencies are shown in Figs. 8 and 9. The gain variation on the XOY plane is less than 1.8 dB, and the gain pattern on this plane demonstrates good omnidirectional characteristics. In addition, a low cross-polarization level of the two polarizations can be observed, which is less than −15 dB. The measured and simulated results are generally consistent. The discrepancy between the measured and simulated values may be attributed to manufacturing tolerances, welding deviations, and non-ideal measurement environments.

Comparison of the proposed method with other methods

Table 1 summarizes the key performance indicators of the proposed algorithm and several multi-objective evolutionary algorithms from the literature. Compared with the traditional genetic algorithm-based approach [25], surrogate model-assisted methods [26, 27] and image mapping topology with twin delayed deep deterministic policy gradient (IMT + TD3) method [28], this method shows better performance in terms of optimization speed and convergence, especially in high-dimensional and multi-objective problems, avoiding the problem of easily falling into local optimality. Compared with the IBPSO and BBSO methods [29, 30], the proposed optimization framework can better cope with the nonlinear relationship between topology and size parameters when dealing with complex antenna structures, thereby achieving more accurate design optimization. Compared with the multi-objective evolutionary algorithm-based methods [31–33], MOEA/D-IHPSO can better handle mixed optimization problems of discrete and continuous variables, provide a more flexible optimization space in antenna design, and maintain good global search capabilities while achieving efficient optimization.

Table 2. Statistics of different algorithm results

Optimization method	Worst	Best	Mean	T. algorithm
IBPSO	2052	1620	1836	141.4 h /run
MOEA/D-GO	1836	1548	1714	130.3 h /run
MOEA/D-IHPSO	1368	1152	1268	96.4 h /run

The mean number of EM simulations and time consumption under 5 independent runs for different algorithms are presented in Table 2. The number of EM simulations for MOEA/D under the worst, best, and mean optimization efficiency is 1368, 1152, and 1268, respectively. Based on the average time over 5 runs, the optimization efficiency of this framework (96.4 hours) is improved by 31.8% and 26% compared to IBPSO (141.4 hours) and MOEA/D-GO (130.3 hours), respectively. These results indicate better computational efficiency and stability for complex antenna optimization problems, while also demonstrating the high accuracy and low error characteristics of the proposed optimization method.

Conclusion

This paper proposes an efficient optimization method for the collaborative optimization of antenna topology and size parameters, which deeply integrates the IHPSO algorithm with the multi-objective evolutionary algorithm and introduces a transfer learning-driven adaptive topology recombination strategy. This approach effectively balances global search and local exploitation, improving optimization efficiency. The optimized dual-polarized omnidirectional antenna exhibits a high isolation of 20 dB within

https://doi.org/10.1017/S1759078726103171 Published online by Cambridge University Press

the 3.3–4.2 GHz operating frequency band, as well as good omnidirectional radiation characteristics and stable gain. Compared with the IBPSO and MOEA/D-GO methods, the proposed optimization framework achieves higher efficiency and requires fewer EM simulations. Both simulation and experimental results show that the MOEA/D-IHPSO algorithm effectively improves convergence speed in multi-objective optimization, which confirms its value for antenna design.

Funding statement. This paper is supported by Yunnan Fundamental Research project (202401AT070351, 202401AT070376, and 202301AV070003), Yunnan Key Laboratory of Computer Technologies Application Open Fund, Yunnan Young Top Talents of Ten Thousands Plan (Shen Tao, Yunren Social Development No. 2018 73), College personnel training project (202101BE070001-008), and partially by the Major Science and Technology Projects in Yunnan Province under Grant (202302AG050009 and 202202AD080013).

Competing interests. The authors declare that they have no conflict of interest or competing interests in relation to this work.

References

1. **Hassan E, Wadbro E and Berggren M** (2014) Topology optimization of metallic antennas. *IEEE Transactions on Antennas and Propagation* **62**(5), 2488–2500.
2. **Liu S, Wang Q and Gao R** (2016) MoM-based topology optimization method for planar metallic antenna design. *Acta Mechanica Sinica* **32**, 1058–1064. https://doi.org/10.1007/s10409-016-0584-0
3. **Wang J, Yang XS, Ding X and Wang BZ** (2017) Antenna radiation characteristics optimization by a hybrid topological method. *IEEE Transactions on Antennas and Propagation* **65**(6), 2843–2854. https://doi.org/10.1109/TAP.2017.2688918
4. **Wang LL, Yang XS and Ma CJ** (2023) An efficient gradient-based hybrid parameter-topology optimization for antenna design. *IEEE Transactions on Antennas and Propagation* **71**(12), 9477–9486. https://doi.org/10.1109/TAP.2023.3316391
5. **Zhu H, Yang XS, Wang J and Wang BZ** (2019) Design of MIMO antenna isolation structure based on a hybrid topology optimization method. *IEEE Transactions on Antennas and Propagation* **67**(10), 6298–6307. https://doi.org/10.1109/TAP.2019.2920295
6. **Hassan E, Scheiner B, Michler F, Berggren M, Wadbro E, Röhrl F, Zorn S, Weigel R and Lurz F** (2020) Multilayer topology optimization of wideband SIW-to-waveguide transitions. *IEEE Transactions on Microwave Theory & Techniques* **68**(4), 1326–1339. https://doi.org/10.1109/TMTT.2019.2959759
7. **Li D, Zhang FS and Ren JH** (2012) A compact tri-band antenna design using boolean differential evolution algorithm. *Progress In Electromagnetics Research C* **32**, 139–149. https://doi.org/10.2528/PIERC12070204
8. **Chen S and Chiu H** (2016) Application of multiobjective topology optimization to miniature ultrawideband antennas with enhanced pulse preservation. *IEEE Antennas and Wireless Propagation Letters* **15**, 842–845. https://doi.org/10.1109/LAWP.2015.2476560
9. **Ghadimi A, Nayyeri V, Khanjarian M, Soleimani M and Ramahi OM** (2020) A systematic approach for mutual coupling reduction between microstrip antennas using pixelization and binary optimization. *IEEE Antennas and Wireless Propagation Letters* **19**(12), 2048–2052. https://doi.org/10.1109/LAWP.2020.3022000
10. **Li R, McNamara D, Wei G and Li J** (2018) Increasing radiation efficiency using antenna shape optimization approach. *IEEE Antennas and Wireless Propagation Letters* **17**(3), 393–396. https://doi.org/10.1109/LAWP.2018.2791585
11. **Lu D, Wang L, Yang E and Wang G** (2018) Design of high-isolation wideband dual-polarized compact MIMO antennas with multiobjective optimization. *IEEE Transactions on Antennas and Propagation* **66**(3), 1522–1527. https://doi.org/10.1109/TAP.2017.2784446
12. **He C, Huang S, Cheng R, Tan KC and Jin Y** (2021) Evolutionary multiobjective optimization driven by Generative Adversarial Networks (GANs). *IEEE Transactions on Cybernetics* **51**(6), 3129–3142. https://doi.org/10.1109/TCYB.2020.2985081
13. **Jia X and Lu G** (2019) A hybrid taguchi binary particle swarm optimization for antenna designs. *IEEE Antennas and Wireless Propagation Letters* **18**(8), 1581–1585. https://doi.org/10.1109/LAWP.2019.2924247
14. **Wu Q, Chen W, Yu C, Wang H and Hong W** (2024) Machine-learning-assisted optimization for antenna geometry design. *IEEE Transactions on Antennas and Propagation* **72**(3), 2083–2095. https://doi.org/10.1109/TAP.2023.3346493
15. **Cui L, Zhang Y, Zhang R and Liu QH** (2020) A modified efficient KNN method for antenna optimization and design. *IEEE Transactions on Antennas and Propagation* **68**(10), 6858–6866. https://doi.org/10.1109/TAP.2020.3001743
16. **Zhu R, Wang J, Han Y, Sui S, Qiu T, Jia Y, Feng M, Wang X, Zheng L and Qu S** (2022) Design of aperture-multiplexing metasurfaces via back-propagation neural network: Independent control of orthogonally-polarized waves. *IEEE Transactions on Antennas and Propagation* **70**(6), 4569–4575. https://doi.org/10.1109/TAP.2022.3140523
17. **Wu Q, Chen W, Yu C, Wang H and Hong W** (2023) Knowledge-guided active-base-element modeling in machine-learning-assisted antenna-array design. *IEEE Transactions on Antennas and Propagation* **71**(2), 1578–1589. https://doi.org/10.1109/TAP.2022.3226343
18. **Dou J, Wei S, Gong H, Chen H, Chen Y, Shen T and Song JA** (2025) A simulation-driven surrogate parallel improved AGA method for the automated design of antenna. *IEEE Antennas and Wireless Propagation Letters* **24**(3), 721–725. https://doi.org/10.1109/LAWP.2024.3514156
19. **Zhang W, Feng F, Liu W, Yan S, Zhang J, Jin J and Zhang QJ** (2021) Advanced parallel space-mapping-based multiphysics optimization for high-power microwave filters. *IEEE Transactions on Microwave Theory & Techniques* **69**(5), 2470–2484. https://doi.org/10.1109/TMTT.2021.3065972
20. **Koziel S and Pietrenko-Dabrowska A** (2019) Performance-based nested surrogate modeling of antenna input characteristics. *IEEE Transactions on Antennas and Propagation* **67**(5), 2904–2912. https://doi.org/10.1109/TAP.2019.2896761
21. **Koziel S and Pietrenko-Dabrowska A** (2021) Expedited acquisition of database designs for reduced-cost performance-driven modeling and rapid dimension scaling of antenna structures. *IEEE Transactions on Antennas and Propagation* **69**(8), 4975–4987. https://doi.org/10.1109/TAP.2021.3074632
22. **Yan S, Zhai X, Ren H and Zhang J** (2024) A low-profile dual-polarized omnidirectional antenna for WLAN/UWB applications. *IEEE Antennas and Wireless Propagation Letters* **23**(5), 1433–1437. https://doi.org/10.1109/LAWP.2024.3358324
23. **Feng B, Li H, Chung KL, Sim CYD and Deng L** (2022) A dual-polarized wideband ceiling-mount antenna with low gain variations and high isolation for 5G Sub-6 GHz applications. *IEEE Transactions on Antennas and Propagation* **70**(9), 8572–8577. https://doi.org/10.1109/TAP.2022.3177519
24. **Wu J, Yang S, Chen Y, Qu S and Nie Z** (2017) A low profile dual-polarized wideband omnidirectional antenna based on AMC reflector. *IEEE Transactions on Antennas and Propagation* **65**(1), 368–374. https://doi.org/10.1109/TAP.2016.2631147
25. **John M and Ammann MJ** (2007) Wideband printed monopole design using a genetic algorithm. *IEEE Antennas and Wireless Propagation Letters* **6**, 447–449. https://doi.org/10.1109/LAWP.2007.891962
26. **Liu B, Akinsolu MO, Song C, Hua Q, Excell P, Xu Q and Huang Y** (2021) An efficient method for complex antenna design based on a self adaptive surrogate model-assisted optimization technique. *IEEE Transactions on Antennas and Propagation* **69**(4), 2302–2315. https://doi.org/10.1109/TAP.2021.3051034
27. **Huang H, Yang X-S and Wang BZ** (2023) Machine-learning-based generative optimization method and its application to an antenna decoupling design. *IEEE Transactions on Antennas and Propagation* **71**(7), 6243–6248. https://doi.org/10.1109/TAP.2023.3270716
28. **Dou J, Gong H, Chen H, Chen Y, Shen T and Song J** (2025) A reinforcement learning-based image mapping-topology optimization for antenna

design. *IEEE Antennas and Wireless Propagation Letters* **24**(7), 1759–1763. https://doi.org/10.1109/LAWP.2025.3546348
29. **Dong J, Li Q and Deng L** (2018) Design of fragment-type antenna structure using an improved BPSO. *IEEE Transactions on Antennas and Propagation* **66**(2), 564–571. https://doi.org/10.1109/TAP.2017.2778763
30. **Aldhafeeri A and Rahmat-Samii Y** (2019) Brain storm optimization for electromagnetic applications: Continuous and discrete. *IEEE Transactions on Antennas and Propagation* **67**(4), 2710–2722. https://doi.org/10.1109/TAP.2019.2894318
31. **Li QQ, Chu QX and Chang YL** (2020) Design of compact high-isolation MIMO antenna with multiobjective mixed optimization algorithm. *IEEE Antennas and Wireless Propagation Letters* **19**(8), 1306–1310. https://doi.org/10.1109/LAWP.2020.2997874
32. **Wang D, Wang G, Lu D, Yang N and Zhang Q** (2022) Design of wideband base station antenna by involving fragment-type structures on dipole arms. *IEEE Antennas and Wireless Propagation Letters* **70**(7), 5953–5958. https://doi.org/10.1109/TAP.2022.3161285
33. **Wang X, Wang G, Wang D and Zhang Q** (2023) Ensemble-learning-based multiobjective optimization for antenna design. *IEEE Transactions on Antennas and Propagation* **71**(2), 1295–1303. https://doi.org/10.1109/TAP.2022.3222076



Jiangling Dou was born in 1985 in Jiangsu Province, China. She received her Ph.D. degree in Electromagnetic Fields and Microwave Technology from Southeast University in 2018. She is currently working at Kunming University of Science and Technology. Her research interests include electromagnetic field theory and applications.



Cailong Zhong was born in 2000 in Jiangxi Province, China. He is currently working toward a graduate degree at the School of Information Engineering and Automation, Kunming University of Science and Technology. His research interests include antenna topology optimization and deep learning.



Dan Li was born in 1999 in Yunnan Province, China. He is currently pursuing a master's degree at Kunming University of Science and Technology.



Jian Song (Member, IEEE) obtained his Bachelor of Engineering degree in Electronics Information Engineering from Jiangxi University of Science and Technology in Ganzhou, China. He later earned his Ph.D. in Electromagnetic Fields and Microwave Technology from the University of Electronic Science and Technology of China in Chengdu in 2015. Between 2015 and 2019, he served as an Algorithm Engineer at Huawei Technology Co., Ltd. in Shenzhen, China. In 2019, he became a faculty member at Kunming University of Science and Technology. His research focuses on microwave engineering and the processing of biomedical images.



Tao Shen (Senior Member, IEEE) earned his Ph.D. from the Illinois Institute of Technology in Chicago, Illinois, USA, in 2013. Presently, he holds the position of President at Yunnan Vocational and Technical College of Mechanical and Electrical Engineering. Dr. Shen has contributed to over 20 publications in prestigious SCIE-indexed journals and leading international conferences within his research domains. His areas of expertise include image processing, artificial intelligence, and the Internet of Energy.

https://doi.org/10.1017/S1759078726103171 Published online by Cambridge University Press